AIP | Applied Physics Letters

Rapid, all-optical crystal orientation imaging of two-dimensional transition metal dichalcogenide monolayers

Sabrina N. David, Yao Zhai, Arend M. van der Zande, Kevin O'Brien, Pinshane Y. Huang, Daniel A. Chenet, James C. Hone, Xiang Zhang, and Xiaobo Yin

Citation: Applied Physics Letters **107**, 111902 (2015); doi: 10.1063/1.4930232
View online: http://dx.doi.org/10.1063/1.4930232
View Table of Contents: http://scitation.aip.org/content/aip/journal/apl/107/11?ver=pdfcov
Published by the AIP Publishing

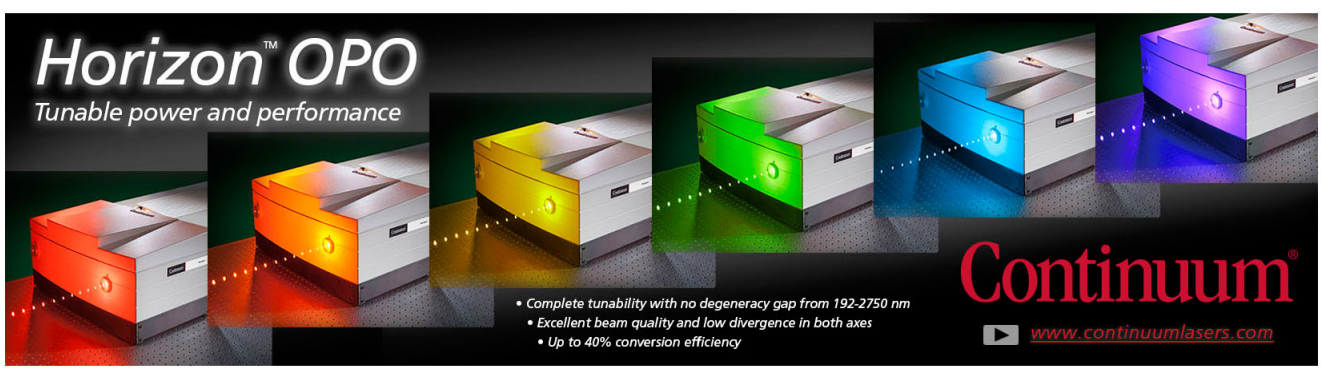

Rapid, all-optical crystal orientation imaging of two-dimensional transition metal dichalcogenide monolayers

Sabrina N. David,[1] Yao Zhai,[2] Arend M. van der Zande,[3,4] Kevin O'Brien,[5] Pinshane Y. Huang,[4] Daniel A. Chenet,[3] James C. Hone,[3] Xiang Zhang,[5,6,7] and Xiaobo Yin[1,2,a)]

[1]*Materials Science and Engineering Program, University of Colorado, Boulder, Colorado 80309, USA*
[2]*Department of Mechanical Engineering, University of Colorado, Boulder, Colorado 80309, USA*
[3]*Department of Mechanical Engineering, Columbia University, New York, New York 10027, USA*
[4]*Department of Mechanical Science and Engineering, University of Illinois, Urbana, Illinois 61801, USA*
[5]*NSF Nanoscale Science and Engineering Center (NSEC), University of California, Berkeley 3112 Etcheverry Hall, UC Berkeley, California 94720, USA*
[6]*Department of Physics, King Abdulaziz University, Jeddah, Saudi Arabia*
[7]*Materials Sciences Division, Lawrence Berkeley National Laboratory, 1 Cyclotron Road, Berkeley, California 94720, USA*

(Received 8 June 2015; accepted 25 August 2015; published online 17 September 2015)

Two-dimensional (2D) atomic materials such as graphene and transition metal dichalcogenides (TMDCs) have attracted significant research and industrial interest for their electronic, optical, mechanical, and thermal properties. While large-area crystal growth techniques such as chemical vapor deposition have been demonstrated, the presence of grain boundaries and orientation of grains arising in such growths substantially affect the physical properties of the materials. There is currently no scalable characterization method for determining these boundaries and orientations over a large sample area. We here present a second-harmonic generation based microscopy technique for rapidly mapping grain orientations and boundaries of 2D TMDCs. We experimentally demonstrate the capability to map large samples to an angular resolution of $\pm 1^\circ$ with minimal sample preparation and without involved analysis. A direct comparison of the all-optical grain orientation maps against results obtained by diffraction-filtered dark-field transmission electron microscopy plus selected-area electron diffraction on identical TMDC samples is provided. This rapid and accurate tool should enable large-area characterization of TMDC samples for expedited studies of grain boundary effects and the efficient characterization of industrial-scale production techniques. © *2015 AIP Publishing LLC*. [http://dx.doi.org/10.1063/1.4930232]

Since the isolation of graphene, an atomically thin carbon membrane, two-dimensional (2D) electronic materials have been extensively investigated for their unique electronic[1–3] and optical[4,5] properties, structural integrity,[6,7] thermoelectric performance,[8] and catalytic function.[9] Large-area samples of transition metal dichalcogenides (TMDCs) in particular, such as MoS_2 and WSe_2, have been highly studied in recent years. Their inherent electronic band gap[10] and polarization-sensitive optical selection rules[11–13] may allow them to be more readily exploited in next-generation electronic and optoelectronic devices. This promise has motivated extensive research into synthesis of large-area TMDC films, with the best results to date achieved by chemical vapor deposition (CVD) methods.[14,15] However, thin film samples are inherently polycrystalline due to the nature of nucleation-based growth, and the presence and type of grain boundaries can affect the electrical, optical, and mechanical properties of monolayers. Carrier scattering has been shown to worsen the conductivity of graphene at boundaries with poor domain connectivity;[16] studies on mechanical strength have found that while tilt-grain boundaries preserve resilience, low-angle boundaries may severely compromise monolayer samples;[17] and in monolayers the photoluminescence at grain boundaries differs significantly from the bulk.[15] Full utilization of these monolayer materials therefore requires an understanding of the effects of the two-dimensional grain structure on material behavior and performance.[18,19] An impediment to both the study of these materials and progress in device fabrication with two-dimensional electronic materials is the time-intensive nature of existing metrology methods for accurately characterizing complete grain boundary and grain orientation information, typically involving dark-field transmission electron microscopy (DF-TEM) in conjunction with filtered electron diffraction. DF-TEM is used to first obtain an image of a single grain, and electron diffraction measurements are then taken on the individual grain. The resulting spot pattern can be carefully interpreted to determine its exact crystal orientation within $\pm 0.5^\circ$ accuracy.[15] While providing highly accurate rotation information and atomic-scale resolution among other benefits, the method is restricted from being applied over relatively large-area samples. Moreover, the 2D atomic material needs to be transferred from its underlying substrate to a TEM grid or an electron-permeable supporting membrane, a time-consuming and invasive process that often requires use of polymers or wet chemicals,[20,21] thermal tapes,[22] or polydimethylsiloxane (PDMS) stamps.[23]

Optical microscopy, on the other hand, allows large-area imaging with moderate spatial resolution. Polarized light microscopy, in particular, provides quantitative information on

a)Author to whom correspondence should be addressed. Electronic mail Xiaobo.Yin@Colorado.Edu.

the crystallographic symmetry of a material and defect or strained regions within it, among other properties. However, optical microscopes do not provide intrinsic contrast sufficient for differentiating grain boundaries within a contiguous two-dimensional atomic film. Selective oxidation of the substrate at crystal boundaries has been used to provide such contrast in graphene grown on copper foils, where it was used to measure the inverse relationship of sheet resistance with increasing graphene grain size.[24] Here, we show that the polarized second-harmonic generation (SHG) from 2D atomic materials allows the rapid mapping of grain boundaries and grain orientations for large-area samples. This technique, which utilizes the inherent second-order nonlinearity of non-centrosymmetric monolayer samples,[25–28] does not require invasive sample preparation nor multi-modality measurements. The nonlinear optical imaging technique allows mapping of arbitrarily large sample regions, shown here for sample regions greater than a square millimeter, in mere seconds and via a single form of measurement, while showing excellent agreement with the orientation information determined using DF-TEM in conjunction with selected-area electron diffraction.

Figure 1 shows an optical image and the all-optical grain mapping on the same millimeter-sized area of an as-grown MoS_2 monolayer. The sample was fabricated by CVD using solid MoO_3 and S precursors on extensively cleaned Si/SiO_2 substrates.[15] In the pure optical image (Fig. 1(b)), the multitude of grain boundaries in the film is completely invisible. Grain colors in Fig. 1(a) represent grain orientations from 0° to 30°, the significance of this angle range being discussed below. Mapping the grain orientations in this millimeter-scale image via the SHG-based optical method is accurate and efficient. An ultrafast Ti:Sapphire laser operated in the infrared was used for excitation of second-harmonic generation. The nonlinear emission was sequentially collected as the sample was confocally scanned point-by-point, and the polarization components of the emission were subsequently discriminated using waveplates and polarizers. With this method, the size of area imaged, image resolution, and

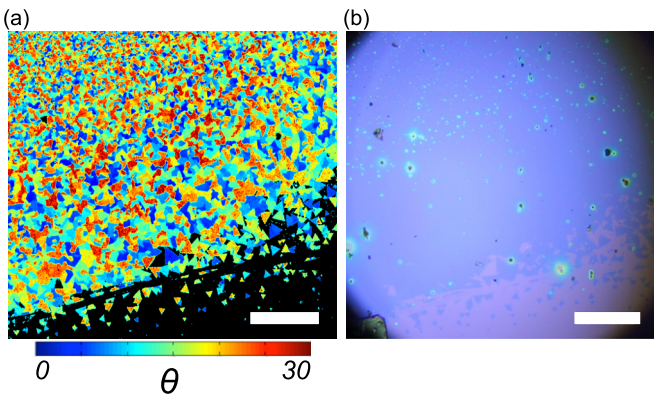

FIG. 1. A 1.2 mm × 1.2 mm area of MoS_2 film with the relative orientations of individual grains color-mapped by SHG microscopy (a) and as seen under a conventional microscope where individual grains within the film are indistinguishable (b). The color-mapped orientation image was produced by two, rapid all-optical SHG scans (with and without a measurement polarizer) performed in reflection geometry with the excitation laser swept through a 10 × 0.3 NA plan fluorite objective, and automated processing. Scale bars 250 μm.

acquisition speed are simply determined by the objective lens magnification and pixel grid choices. No modification of method nor special sample preparation is required to map the orientations of monolayer islands on a background substrate, continuous films, or regions with both continuous film and flakes (as seen in Fig. 1); it can be flexibly applied to samples in various stage of growth and of unknown types. Requisite laser power for mapping a given sample can depend on factors such as film quality and pump wavelength, where appropriate excitation wavelengths are material-dependent and in these studies have ranged from 800 nm to 1300 nm. Fig. 1 was obtained with less than 200 mW at the microscope entrance.

The grain orientation information in the images acquired with this all-optical technique is enabled by the inherent non-centrosymmetricity of monolayer TMDCs. In non-centrosymmetric materials, a second-order polarization can be induced by incident electromagnetic fields, $P^{(2)}_{2\omega} = \chi^{(2)}_{ijk} : E_\omega E_\omega$, where $\chi^{(2)}_{ijk}$, the second-order susceptibility tensor of the material, respects the same underlying symmetry as the material crystal lattice and governs the relationship between the induced second-harmonic polarization $P^{(2)}_{(2\omega)}$ and the incident field E_ω. The intensity of radiated second-harmonic emission having a given polarization $\hat{e}_{2\omega}$ from these monolayers is given by:[25] $I_{2\omega} = |\hat{e}_{2\omega}.(\chi^{(2)}_{ijk}.\hat{e}_\omega).\hat{e}_\omega|^2$. For materials in the *D3h* point group, such as the monolayer TMDCs, the third rank tensor $\chi^{(2)}_{ijk}$ has only four non-zero elements: $\chi = \chi^{(2)}_{112} = \chi^{(2)}_{121} = \chi^{(2)}_{211} = -\chi^{(2)}_{222}$. To determine how the angular orientation of a grain will affect the polarization of emitted SHG, a two-dimensional crystal oriented at an arbitrary angle θ relative to the axis of polarization of an incident pump signal can be considered. In this system, the $\chi^{(2)}_{ijk}$ tensor should be transformed by a rotation through the angle θ, and the above expression for SHG intensity ($I_{2\omega}$) evaluated with $\hat{e}_\omega$ defined as the x or y coordinate axis. It follows that the intensity of two orthogonal output second-harmonic polarizations for excitation and collection at normal incidence takes the form: $I^x_{2\omega} = |\chi^{(2)}\cos(3\theta)|^2$ and $I^y_{2\omega} = |\chi^{(2)}\sin(3\theta)|^2$. Figure 2(a) plots the polarized SHG intensity dependence on grain rotation angle for a *D3h* sample, showing symmetric power peaks at 60° separation. Grain orientation mapping (Fig. 2(b)) entails simple image processing of an x-polarized intensity (Fig. 2(c)) and y-polarized intensity image (Fig. 2(d)): $\theta = \frac{1}{3}\tan^{-1}\left(\sqrt{I^y_{2\omega}}/\sqrt{I^x_{2\omega}}\right)$. The x and y coordinates represent the directions of the orthogonal polarizers for the output SHG signal and can be any direction relative to the primitive MoS_2 lattice or incident polarization as long as they are orthogonal to one another. Grain boundaries invisible in the conventional optical image (e.g., Fig. 1(b)) become clearly visible, and orientation information is straightforwardly displayed. Grain color corresponds to angular orientation, with the color scale representing relative angles between 0° and 30°.

The measureable angle range using intensity measurement as performed above is 0° and 30° due to the reflection symmetry of the MoS_2 lattice in conjunction with the 6-fold symmetry present without phase information. In DF-TEM,

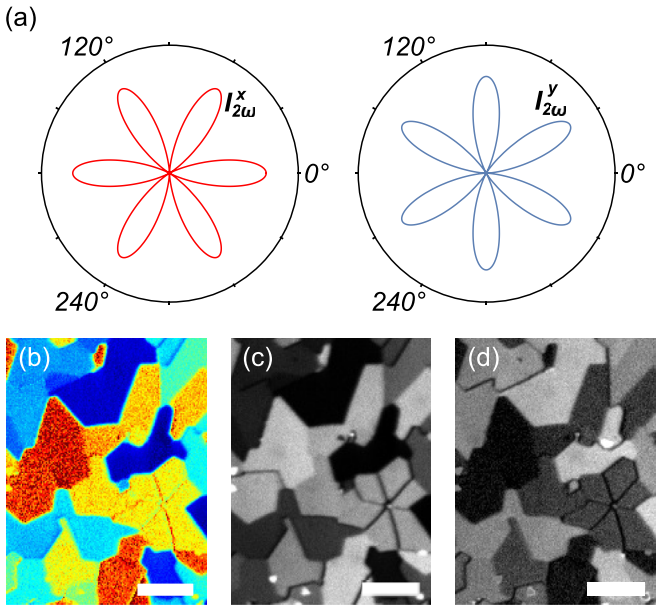

FIG. 2. (a) A polar plot showing the theoretical angular dependence of *x*-polarized (blue) and *y*-polarized (red) output SHG intensity through 2π rotation of a sample from the *D3h* point symmetry with 6-fold rotational symmetry. The pump beam is also defined to have *x*-direction polarization. The angular polarized SHG intensity dependence is used to determine crystallographic orientation from measured SHG intensity. (b) A grain orientation map of a high-quality TMDC sample. Color bar from Fig. 1 applies. (c) The *x*- and (d) *y*-polarized SHG images processed to produce the orientation map in (b) by $\theta = \frac{1}{3}\tan^{-1}\left(\sqrt{I^y_{2\omega}}/\sqrt{I^x_{2\omega}}\right)$. Scale bars 25 μm.

the 6-fold rotational symmetry is reduced to true three-fold symmetry of the lattice by differences in scattering brightness by the Mo and S sublattices.[15] In this optical method, the exact angle (e.g., 0° and 120°) of grains can be unambiguously determined by considering phase. For example, angular mismatch between adjacent grains becomes implicit in the darkness of shared boundaries in a non-polarized, intensity image; opposite orientations such as $[\bar{1}110]$ and $[1\bar{1}10]$ must emit SHG signals that are exactly out of phase while slightly misaligned grains will have only a small phase difference in SHG emissions. While the microscope objective, beam splitters, lenses, and other optical components will introduce additional phase differences between SHG signals of different polarizations, accurate discrimination of the relative phases of different polarizations can be accomplished by careful compensation, e.g., with signal retarders or similar methods. Phase-sensitive SHG[29] provides complete information for direct calculation of grain angle.

We examine the accuracy of this method by direct comparison to a complete DF-TEM plus selected area electron-diffraction characterization of a high-quality TMDC sample.[16] Figure 3 shows nonlinear optical grain orientation maps of two 500 μm × 500 μm MoS_2 samples, primarily monolayer triangular islands, ranging in size from 20 μm to 120 μm, fabricated by seed-free CVD.[15] In Figure 3, subsets of crystal grains mapped by our all-optical characterization (d) and (f) are compared with the corresponding results from diffraction-filtered DF-TEM (c) and (e). The color map of the SHG images represents angles ranging from 0° to 30°. In the DF-TEM images, flakes have been colored post-analysis so that flakes of different orientations have different colors

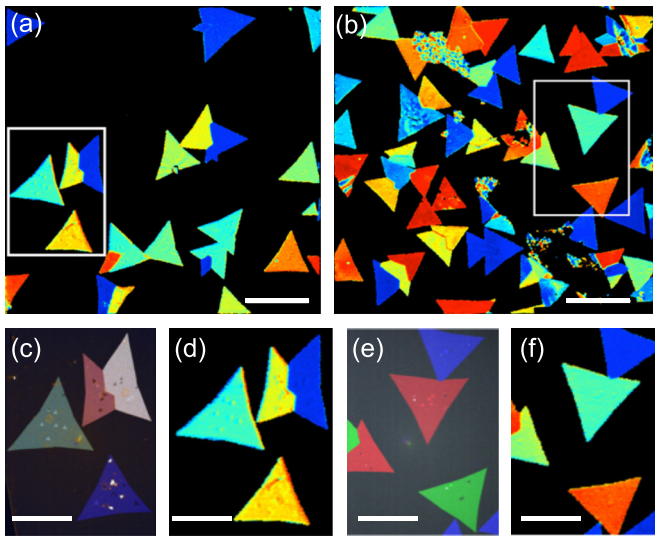

FIG. 3. Grain orientation maps of two 500 μm × 500 μm samples containing primarily monolayer MoS_2 triangular islands ranging in size from 20 μm to 120 μm generated by all-optical SHG microscopy (a) and (b) with 20 × 0.45 NA plan fluorite objective and point-by-point piezo-actuated translation of the sample. Scale bars 100 μm. Comparison of the grain orientation color maps from the insets of (a) and (b) between the SHG-based microscopy method (d) and (f) and corresponding DF-TEM results (c) and (e). Color bar of Fig. 1 applies. Scale bars 60 μm.

(and those with the same orientation share the same color). Good agreement is seen between the methods. In Figs. 3(e) and 3(f), sets of grains shown to have the same orientation are consistent across both methods. In both cases, a very slight difference between two of the central grains, i.e., the two red-colored grains in Fig. 3(e) or cyan- to yellow-colored grains in Fig. 3(f), is also visible. In Figs. 3(c) and 3(d), both methods of mapping show all four grains in this subset having different orientations. The joined grains in the upper right of the subset of Figs. 3(c) and 3(d) are shown having mismatched orientations and a boundary that tracks well between the two methods. The measured angle difference between these joined grains by selected-area electron diffraction is 40° ± 0.5°. See Ref. 15 for detailed information on the DF-TEM measurement of these grains. The all-optical method here also supports 40° separation between the joined grains: within the 30° angle range automatically displayed by the imaging system a 20° angle is shown, which can be any of the symmetry equivalents: 20°, 40°, 80°, or 100°. As discussed above, phase-sensitive measurement can

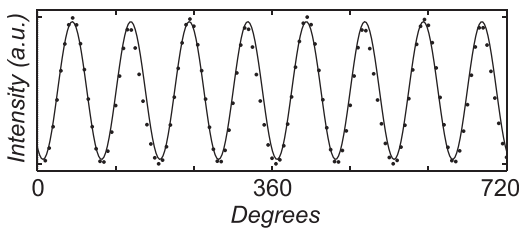

FIG. 4. Polarization-dependent intensity data for rotation of a *D3h* sample through 720° fit with a sinusoidal curve. A least-squares method is used for the sinusoidal fit, the period and character of which is derived from the $\chi^{(2)}_{ijk}$ tensor. From the quantified error in experimental fit, a resolution of ±1.12° is determined for the measurement method.

narrow the number of symmetry equivalents to two (60° apart), and the boundary darkness in unpolarized images unambiguously determines which is accurate for adjacent grains. While here the measurement is performed without a phase reference, we simply show that the rapidly processed SHG images provide accurate angle information based on comparison to DF-TEM.

This all-optical grain-mapping technique provides resolution comparable to that achieved by TEM methods. Figure 4 shows polarization-dependent intensity data collected through two full rotations of the measurement polarizer, e.g., 720°, fit with a sinusoidal curve according to theory-based dependence on polarization angle of a rotated measurement polarizer. The angular resolution of this all-optical method is ±1.12°, as determined by the 95% confidence bounds for the theory-based fit to the sinusoidal experimental data. Angular resolution may improve with additional measurements, e.g., further rotations of the output polarizer. The spatial resolution presented here ranges from approximately 0.62 μm (Fig. 2) to 1 μm (Figs. 1 and 3) and can be improved by use of higher numerical aperture objectives. With this resolution, the location of grain boundaries is clear from the angular differences in adjacent SHG emissions. Potential SHG effects of localized bilayers or multilayers at the grain boundaries[30] are not recorded and would require methods of higher resolution, such as near-field nonlinear optical microscopy. Generally, the SHG response from bilayers is expected to be dark, and from higher level multilayers alternately bright and dark according to odd and even numbers of layers.[25–28]

In summary, the demonstrated SHG-based microscopy method allowed grain orientation maps to be acquired in minutes with a single measurement modality, no sample preparation, and fast automated analysis. Comparison to DF-TEM plus selected-area electron diffraction shows the orientation information to be highly accurate. While the results derived above are specific to materials in the *D3h* point group, this method can easily be extended to other materials in other noncentrosymmetric groups as SHG characteristics of the different point groups relevant for the analysis derived above are well-known.[31] The capabilities demonstrated herein are promising for rapid and even real-time mapping of monolayer flakes and grains for experimental and industrial processes.

This work was partially supported by the Soft Materials Research Center under NSF MRSEC Grant No. DMR-1420736 and the University of Colorado. A.v.d.Z., D.C., and J.H. were supported by the NSF Grant No. DMR-1124849 and by Air Force Office of Scientific Research (AFOSR) FA9550-14-1-0268. K.O. and X.Z. were supported by the 'Light-Material Interactions in Energy Conversion' Energy Frontier Research Center funded by the U.S. Department of Energy, Office of Science, Office of Basic Energy Sciences under Award Number DE-AC02-05CH11231.

[1]A. K. Geim and K. S. Novoselov, Nat. Mater. **6**, 183 (2007).
[2]C. Ataca, H. Sahin, E. Aktürk, and S. Ciraci, J. Phys. Chem. C **115**, 3934 (2011).
[3]B. Radisavljevic, A. Radenovic, J. Brivio, V. Giacometti, and A. Kis, Nat. Nanotechnol. **6**, 147 (2011).
[4]A. Splendiani, L. Sun, Y. Zhang, T. Li, J. Kim, C.-Y. Chim, G. Galli, and F. Wang, Nano Lett. **10**, 1271 (2010).
[5]K. F. Mak, C. Lee, J. C. Hone, J. Shan, and T. F. Heinz, Phys. Rev. Lett. **105**, 136805 (2010).
[6]C. Lee, X. Wei, J. W. Kysar, and J. C. Hone, Science **321**, 385 (2008).
[7]S. Bertolazzi, J. Brivio, and A. Kis, ACS Nano **5**, 9703 (2011).
[8]X. Liu, G. Zhang, Q. X. Pei, and Y. W. Zhang, Appl. Phys. Lett. **103**, 133113 (2013).
[9]Y. Li, H. Wang, L. Xie, Y. Liang, G. Hong, and H. Dai, J. Am. Chem. Soc. **133**, 7296 (2011).
[10]S. Lebègue and O. Eriksson, Phys. Rev. B **79**, 115409 (2009).
[11]T. Cao, G. Wang, W. Han, H. Ye, C. Zhu, J. Shi, Q. Niu, P. Tan, E. Wang, B. Liu, and J. Feng, Nat. Commun. **3**, 887 (2012).
[12]W. Yao, D. Xiao, and Q. Niu, Phys. Rev. B **77**, 235406 (2008).
[13]H. Zeng, J. Dai, W. Yao, D. Xiao, and X. Cui, Nat. Nanotechnol. **7**, 490 (2012).
[14]Y.-H. Lee, X.-Q. Zhang, W. Zhang, M.-T. Chang, C.-T. Lin, K.-D. Chang, Y.-C. Yu, J. T.-W. Wang, C.-S. Chang, L.-J. Li, and T.-W. Lin, Adv. Mater. **24**, 2320 (2012).
[15]A. M. van der Zande, P. Y. Huang, D. A. Chenet, T. C. Berkelbach, Y. You, G.-H. Lee, T. F. Heinz, D. R. Reichman, D. A. Muller, and J. C. Hone, Nat. Mater. **12**, 554 (2013).
[16]A. W. Tsen, L. Brown, M. P. Levendorf, F. Ghahari, P. Y. Huang, R. W. Havener, C. S. Ruiz-Vargas, D. A. Muller, P. Kim, and J. Park, Science **336**, 1143 (2012).
[17]R. Grantab, V. B. Shenoy, and R. S. Ruoff, Science **330**, 946 (2010).
[18]P. Y. Huang, C. S. Ruiz-Vargas, A. M. van der Zande, W. S. Whitney, M. P. Levendorf, J. W. Kevek, S. Garg, J. S. Alden, C. J. Hustedt, Y. Zhu, J. Park, P. L. McEuen, and D. A. Muller, Nature **469**, 389 (2011).
[19]G.-H. Lee, R. C. Cooper, S. J. An, S. Lee, A. M. van der Zande, N. Petrone, A. G. Hammerberg, C. Lee, B. Crawford, W. Oliver, J. W. Kysar, and J. C. Hone, Science **340**, 1073 (2013).
[20]S. Najmaei, Z. Liu, W. Zhou, X. Zou, G. Shi, S. Lei, B. I. Yakobson, J.-C. Idrobo, P. M. Ajayan, and J. Lou, Nat. Mater. **12**, 754 (2013).
[21]W. Regan, N. Alem, B. Alemań, B. Geng, C. Girit, L. Maserati, F. Wang, M. Crommie, and A. Zettl, Appl. Phys. Lett. **96**, 113102 (2010).
[22]J. D. Caldwell, T. J. Anderson, J. C. Culbertson, G. G. Jernigan, K. D. Hobart, F. J. Kub, M. J. Tadjer, J. L. Tedesco, J. K. Hite, M. A. Mastro, R. L. Myers-Ward, C. R. Eddy, P. M. Campbell, and D. K. Gaskill, ACS Nano **4**, 1108 (2010).
[23]K. S. Kim, Y. Zhao, H. Jang, S. Y. Lee, J. M. Kim, K. S. Kim, J.-H. Ahn, P. Kim, J.-Y. Choi, and B. H. Hong, Nature **457**, 706 (2009).
[24]D. L. Duong, G. H. Han, S. M. Lee, F. Gunes, E. S. Kim, S. T. Kim, H. Kim, Q. H. Ta, K. P. So, S. J. Yoon, S. J. Chae, Y. W. Jo, M. H. Park, S. H. Chae, S. C. Lim, J. Y. Choi, and Y. H. Lee, Nature **490**, 235 (2012).
[25]X. Yin, Z. Ye, D. A. Chenet, Y. Ye, K. O'Brien, J. C. Hone, and X. Zhang, Science **344**, 488 (2014).
[26]M. A. van der Veen, F. Vermoortele, D. E. De Vos, and T. Verbiest, Anal. Chem. **84**, 6378 (2012).
[27]N. Kumar, S. Najmaei, Q. Cui, F. Ceballos, P. M. Ajayan, J. Lou, and H. Zhao, Phys. Rev. B **87**, 161403 (2013).
[28]Y. Li, Y. Rao, K. F. Mak, Y. You, S. Wang, C. R. Dean, and T. F. Heinz, Nano Lett. **13**, 3329 (2013).
[29]A. Savoia, D. Paparo, P. Perna, Z. Ristic, M. Salluzzo, F. Miletto Granozio, U. Scotti di Uccio, C. Richter, S. Thiel, J. Mannhart, and L. Marrucci, Phys. Rev. B **80**, 075110 (2009).
[30]Z. Liu, M. Amani, S. Najmaei, Q. Xu, X. Zou, W. Zhou, T. Yu, C. Qiu, A. G. Birdwell, F. J. Crowne, R. Vajtai, B. I. Yakobson, Z. Xia, M. Dubey, P. M. Ajayan, and J. Lou, Nat. Commun. **5**, 5246 (2014).
[31]T. F. Heinz, M. M. T. Loy, and W. A. Thompson, Phys. Rev. Lett. **54**, 63 (1985).